

AutoMerge: A Framework for Map Assembling and Smoothing in City-scale Environments

Peng Yin^{1,*}, *Member, IEEE*, Haowen Lai^{2,+}, Shiqi Zhao^{3,+}, Ruijie Fu¹, Ivan Cisneros¹, Ruohai Ge¹, Ji Zhang¹, Howie Choset¹, *Fellow, IEEE*, and Sebastian Scherer¹, *Senior Member, IEEE*

Abstract—We present AutoMerge, a LiDAR data processing framework for assembling a large number of map segments into a complete map. Traditional large-scale map merging methods are fragile to incorrect data associations, and are primarily limited to working only offline. AutoMerge utilizes multi-perspective fusion and adaptive loop closure detection for accurate data associations, and it uses incremental merging to assemble large maps from individual trajectory segments given in random order and with no initial estimations. Furthermore, after assembling the segments, AutoMerge performs fine matching and pose-graph optimization to globally smooth the merged map. We demonstrate AutoMerge on both city-scale merging (120km) and campus-scale repeated merging (4.5km×8). The experiments show that AutoMerge (i) surpasses the second- and third- best methods by 14% and 24% recall in segment retrieval, (ii) achieves comparable 3D mapping accuracy for 120 km large-scale map assembly, (iii) and it is robust to temporally-spaced revisits. To the best of our knowledge, AutoMerge is the first mapping approach that can merge hundreds of kilometers of individual segments without the aid of GPS.

Index Terms—Map Merging, Viewpoint-invariant Localization, Multi-agent SLAM, Incremental Mapping, GPS-denied

I. SYSTEM OVERVIEW

As shown in Fig. 1, AutoMerge provides an automatic map merging system for the large-scale single-/multi- agent mapping task. Each agent is equipped with a LiDAR mapping module to enable self-maintained sub-map generation and odometry estimation. The AutoMerge system consists of three modules: 1) fusion-enhanced place descriptor extraction, 2) an adaptive data-association mechanism to provide high accuracy and recall for segment-wise place retrievals, and 3) a partially decentralized system to provide centralized map merging and single agent self-localization in the world frame.

Fusion-enhanced Descriptor: Each agent runs the decentralized mapping sub-system as an extension of LiDAR-inertial odometry estimation [40], which also provides a sub-map extraction module for onboard adaptive descriptor extraction. Such a descriptor has the following advantages: 1) it is translation-invariant due to the local translation-equivalent property of 3D point-clouds [14], 2) it is orientation-invariant

due to the rotation-equivalent property of spherical harmonics [5], and 3) it is light-weight compared to the original raw sub-maps. Thus, a single agent can provide paired viewpoint-invariant place descriptors and ego-motion to the AutoMerge server system through lower bandwidth communication.

Adaptive Loop Closure Detection: Spurious loop closures are frequent in environments with repetitive appearances, such as long streets. On the one hand, false positive place retrievals may easily break the global optimization system, and ideally 100% accuracy can avoid these optimization failures for large-scale mapping. On the other hand, low recalls can provide partial data association, which will affect global optimization performance. Hybrid loop closure detection takes advantage of sequence matching to provide continuous true positive retrievals over long overlaps, and RANSAC-based single frame detection for local overlaps. By analysing the feature correlation between segments, we can balance the place retrievals from sequence-/single- frame matching to provide accurate retrievals for offline/online LCD.

Incremental Merging: Traditional centralized map merging [1] is usually reliant on initial relative odometry estimation and geometry-based point cloud registration. Such methods are very sensitive to odometry drifts. In contrast, AutoMerge can use the paired place descriptors and ego-motions of each agent to capitalize on loop closure opportunities (high accuracy and recall) for correction, despite a large amount of odometric drift. Using this hybrid loop closure detection method, AutoMerge performs a rough centralized global map optimization **GO**. In the **Rough Merge** step, AutoMerge picks one segment as the root node, and transforms other segments onto the existing nodes based on their keyframe associations and ICP-based local map alignments. The disadvantage of descriptor-based data association is the low accuracy, since it ignores the true transformation between segments. In the **Refine Merge** step, AutoMerge calculates the accurate transform via geometry-based point cloud registration for all paired overlaps, and utilizes a factor-graph to refine the final merged results. After merging, each agent can optimize its localization, **LO**, through **GO** and their own odometry estimation.

In offline map merging, AutoMerge can detect all of the potential matches between all of the segments, and directly merge sub-maps into a global map along high confidence overlaps. In online map merging, the AutoMerge server can incrementally accumulate the key-frames and corresponding poses, and merges segments with strong connections.

Peng Yin, Ruijie Fu, Ivan Cisneros, Ruohai Ge, Ji Zhang, Howie Choset, and Sebastian Scherer are with the Robotics Institute, Carnegie Mellon University, Pittsburgh, PA 15213, USA. {hitmaxtom@gmail.com, (ruijief, icisnero, ruohaig, zhangji, choset, basti}@andrew.cmu.edu}.

Haowen Lai is with the Department of Automation, Tsinghua University, Beijing, China. (lhwl9@mails.tsinghua.edu.cn)

Shiqi Zhao is with University of California San Diego, La Jolla, CA 92093, USA. (s2zhao@eng.ucsd.edu).

*Corresponding author: Peng Yin (hitmaxtom@gmail.com)

+Authors Haowen Lai and Shiqi Zhao contributed equally to this paper.

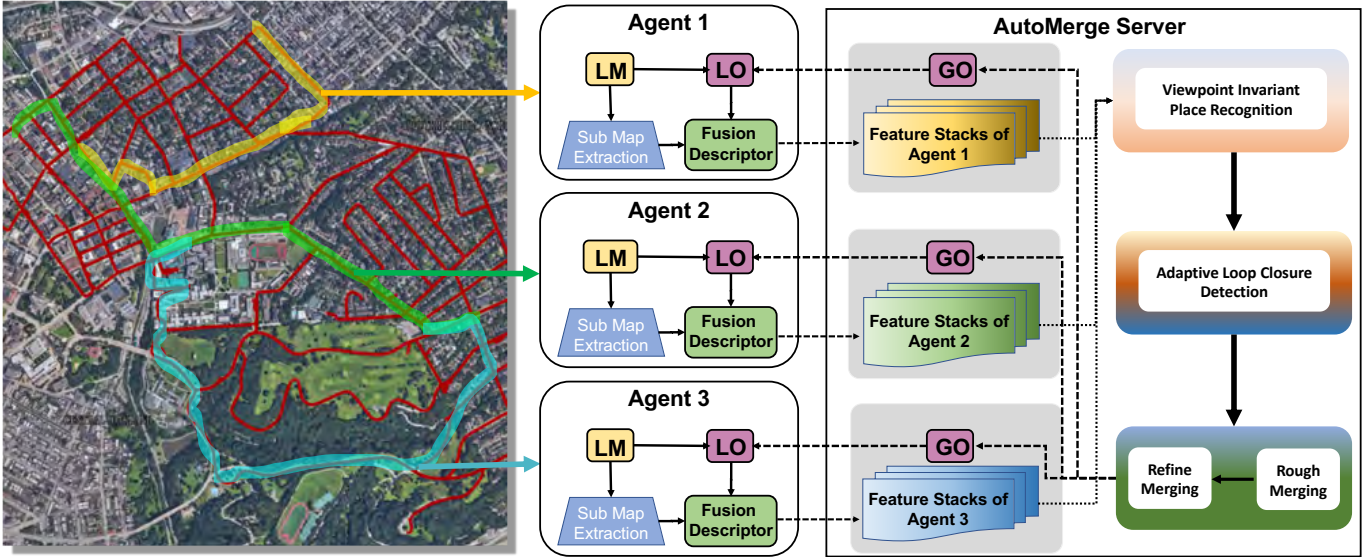


Fig. 1. **AutoMerge system framework.** AutoMerge supports both offline and online global map merging tasks. In the offline mode, AutoMerge can use the previously-stored sub-maps for direct global data association and map merging. In the online mode, given LiDAR odometry estimates, each agent can extract adaptive place descriptors from local sub-maps and stream them back to the AutoMerge Server. Due to the viewpoint-invariance of these descriptors, AutoMerge can estimate accurate data associations between different segments with less recall. The sub-maps are merged into a global map using a global optimization method (GO), and each agent can estimate in parallel their global location through a local optimization (LO) method.

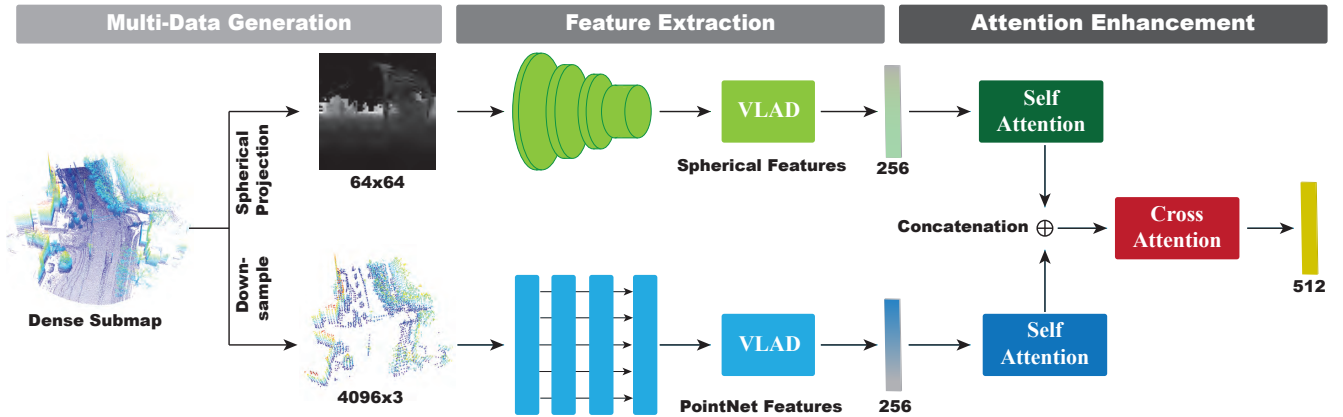


Fig. 2. **The network structure of the AutoMerge descriptor extraction.** To provide viewpoint-invariant descriptor extraction, our network includes a point-based branch to improve the robustness to translation differences, and a sphere-based branch for rotation differences. Finally, AutoMerge utilizes a deep fusion mechanism between the two branches, which can enhance the individual branches and the joint branch simultaneously.

II. FUSION-ENHANCED DESCRIPTOR EXTRACTION

As analyzed in Sec. ??, point-based approaches show better performance against translation differences when compared with projection-based methods, whereas projection-based methods show better accuracy against orientation differences. Our fusion-enhanced descriptor balances the advantages of both point- and projection- based approaches with a multi-perspective feature extraction network. As shown in Fig. 2, the network includes two core components: 1) a multi-perspective feature extraction module, and 2) an attention place feature fusion module.

A. Multi-perspectives Feature Extraction

Due to the sparsity and occlusion problems of a raw LiDAR scan, a 3D observation will vary when gathered under dif-

ferent viewpoints. To provide stable multi-perspective feature extraction, we first accumulate the point cloud into local dense maps. This mechanism can provide a consistent local dense map based on LiDAR odometry estimation, which has been explained in detail in our previous work [6]. In the following subsections, we provide details on how we utilize point-based and projection-based feature extraction in our method.

Point-based Feature Extraction: In this branch, we adopt the idea of PointNetVLAD [3] to extract the global descriptor. Given a local dense map, we query the points set $P = \{p_1, \dots, p_N | p_n \in \mathbb{R}^3\}$ within a $80m \times 80m$ bounding box and preprocess it as shown in [3]. Then, P is fed into PointNet [26] to extract local features $F_p = \{f_1, \dots, f_N | f_n \in \mathbb{R}_p^C\}$. With the help of a NetVLAD layer [27], the global descriptor V_{point}

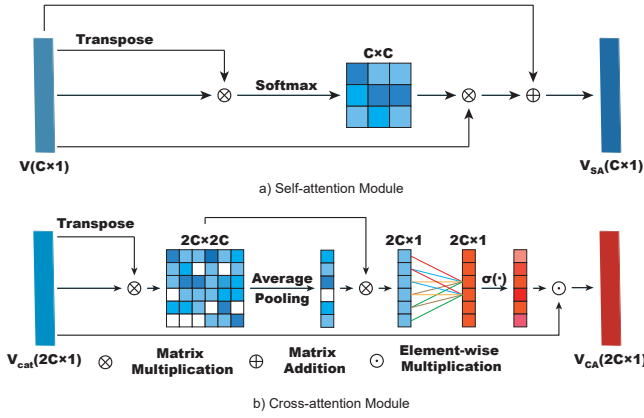


Fig. 3. **Attention-enhanced Feature Extraction.** For each branch, AutoMerge applies a self-attention layer to improve the network feature extraction. Between the two branches, AutoMerge also applies a cross-attention layer to enhance their inner connections.

is obtained by aggregating local point features. Finally, the global descriptor V_{point} is run through a fully connected layer to yield a compact descriptor.

Projection-based Feature Extraction: To obtain viewpoint invariance, we utilize the spherical convolution [31] to extract local features from a spherical projection of the point cloud. Using the local dense maps, we query the points within a range of $50m$ and project them into a panorama using the method mentioned in [6]. Then the corresponding spherical projection $SP \in \mathbb{R}^{H \times W}$ is fed into 4 layers of spherical convolutions to generate local features $F_s \in \mathbb{R}^{C_s \times \alpha \times \beta \times \gamma}$ which contain features sampled from angles in all three axes. A NetVLAD [27] layer is used to find the spatial similarities between local features and reorder them in a specific manner. Finally, the global descriptor V_{sphere} is also run through a fully connected layer to reduce the feature dimensions.

B. Attention Fusion

Our attention fusion module consists of two self-attention modules providing contextual information for V_{point} and V_{sphere} individually, and a cross attention module which aims to reweigh the importance of channels within the concatenation of V_{point} and V_{sphere} .

Self-attention Feature Enhancement: Each channel of the global descriptor can be interpreted as a specific response and different combinations of channels can be regarded as different patterns of the environment [41]. However, when extracting the local features, PointNet [26] only considers each point independently and the receptive field of the spherical convolution is also limited by the number of layers, which leads to a lack of inter-channel dependencies in global descriptors. By exploring the inter-dependencies between channels, we can therefore enhance the semantic information representation of the global descriptor.

$$V_{SA} = V + \gamma \text{SoftMax}(VV^T)^T V \quad (1)$$

Given a global descriptor $V \in \mathbb{R}^{C \times 1}$, we obtained the attention map $A \in \mathbb{R}^{C \times C}$ by directly multiplying V and its transpose and applying a SoftMax function on the result along the row direction. Each element A_{ji} represents the impact of j^{th} channel on i^{th} channel. Then, we multiply the transpose of attention map A with V to generate a weighted sum of every channel which contains the inter-channel dependencies. Finally, we multiply the result with a learnable parameter γ to scale the inter-channel dependencies and add it with V .

Cross-attention Feature Reweighing: While inter-channel dependencies can provide contextual information, they can also evaluate the contribution of each channel. During feature fusion, there are situations that are only beneficial to one of the branches, and so simple concatenation of the two global descriptors will lead to a large performance decrease. Inspired by [42], our cross-attention feature reweighing module learns the inter-channel dependencies and emphasizes the more meaningful channels and neglects the irrelevant channels.

The network structure is illustrated in Fig.3. The input is concatenation of two global descriptor $[V_{point}, V_{sphere}]$ denoted as $V_{cat} \in \mathbb{R}^{2C \times 1}$. We directly get the correlation matrix E from multiplication of V_{cat} and its transpose.

$$E = V_{cat} V_{cat}^T \quad (2)$$

Then, we average the elements in each row of the E to aggregate the responses of each channel, and multiply E with the result to obtain channel correlation weight α_{corr} . We further utilize a fully connected layer to exploit the dependencies of channels and apply a Sigmoid function to narrow the channel importance weight α_w within $[0, 1]$.

$$\alpha_{corr} = E \otimes \text{Ave_Pool}(E) \quad (3)$$

$$\alpha_w = \text{Sigmoid}(W(\alpha_{corr})) \quad (4)$$

Finally, we apply an element-wise multiplication between channel importance weight α_w and V_{cat} to yield the attention-reweighed global descriptor.

$$V_{CA} = \alpha_w \odot V_{cat} \quad (5)$$

C. Learning Metrics

To enable end-to-end training for our network, we utilize the "Lazy quadruplet" loss metric. Sets of training tuples are selected from the training dataset and each of these training tuples is composed of four components: $\mathcal{S} = [S_a, \{S_{pos}\}, \{S_{neg}\}, S_{neg}^*]$, where the S_a represents the query frame location at the ground truth position, $\{S_{pos}\}$ stands for a set of "positive" frames whose distance to S_a is less than the threshold D_{pos} , $\{S_{neg}\}$ denotes a set of "negative" frames whose distance to S_a is strictly larger than threshold D_{neg} and S_{neg}^* represents a frame whose distance to $\{S_{neg}\}$ is strictly larger than D_{neg} . In our case, these two thresholds are set as $D_{pos} = 10m$ and $D_{neg} = 50m$. The lazy quadruplet loss is defined as

$$L_{lazyQuad}(\mathcal{S}) = \max_{i,j}([\gamma + \delta_{pos_i} - \delta_{neg_j}]_+) + \max_{i,k}([\alpha + \delta_{pos_i} - \delta_{neg_k}^*]_+) \quad (6)$$

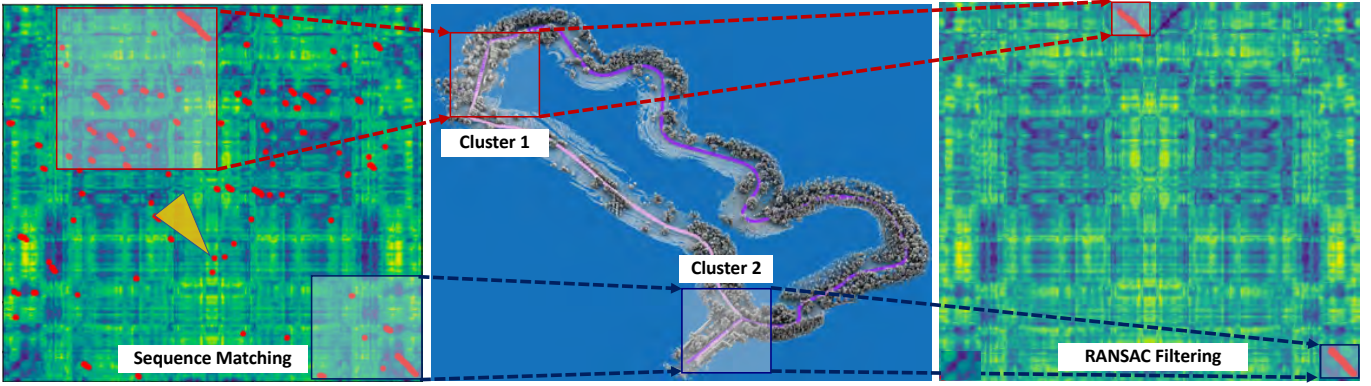


Fig. 4. **Illustration of Adaptive Loop Closure Detection.** (i) The figure shows the difference matrix between two segments, where the red points indicate the potential matches via sequence matching [10] shown in yellow. (ii) The matches are clustered into individual zones via K-means based on their feature distances. (iii) RANSAC is utilized to exclude outliers that can not satisfy Euclidean constraints.

where α and β are the constant threshold giving the margin and $[\dots]_+$ denotes the hinge loss.

III. ADAPTIVE LOOP CLOSURE DETECTION

In our AutoMerge framework, loop closures are required to be accurate (few false positives) and robust (high recall), though these two properties are contradictory. As shown in Fig. 4, our adaptive loop closure detection module can estimate the stable data-association while ignoring the potential outliers, through our sequence matching and RANSAC filtering mechanisms. In this section, we will introduce details.

A. Adaptive Candidates Association

In order to find possible loops among multiple segments, they are grouped into pairs for every two segments T_i and T_j ($i \neq j$). Each T_i has point cloud sub-maps separated by a constant distance and the corresponding poses $\mathbf{T}_i = \{\mathbf{T}_i^k\}$, both of which are obtained from the odometry. These sub-maps are then encoded with our fusion-enhanced descriptor and represented as feature $\mathbf{f}_i = \{\mathbf{f}_i^k\}$. The similarity of places (i.e. sub-maps) of different segments can be revealed in the difference matrix $\mathbf{D} = \mathbf{d}(\mathbf{f}_i, \mathbf{f}_j) \in \mathbb{R}^{N_i \times N_j}$, where $\mathbf{d}(\cdot)$ is the cosine distance and N_i and N_j are the number of sub-maps in T_i and T_j respectively.

Our adaptive LCD method works on loop candidates $\mathcal{C} = \{(k_i, k_j)\}$ where k_i and k_j are the index of submaps in T_i and T_j , showing the association of places in a segment pair. We acquire \mathcal{C}_{seq} by applying sequence matching [10] on the difference matrix \mathbf{D} . However, as we can see in Fig. 4, the raw match result still exists lots outliers. To filter them out, we utilize kmeans to cluster the potential matches into different zones $\mathcal{C}_{\text{seq}_i}, i = 1, \dots, k$ via k-means based on the feature distances. Then for i -th zone, we adopt the idea of RANSAC to select correspondences from $\mathcal{C}_{\text{seq}_i}$, with an edge-based geometric consistency principle to check the correctness of the proposal of correspondences. Specifically, within each iteration, the relation

$$\|\text{edge}_i\|_2 \geq \beta \|\text{edge}_j\|_2, \quad \|\text{edge}_j\|_2 \geq \beta \|\text{edge}_i\|_2 \quad (7)$$

is checked between n samples (k_i, k_j) , where the edges are formed by every two samples (k_i^1, k_j^1) and (k_i^2, k_j^2) , and $\beta \in [0, 1]$ controls the degree on equality of edge length. Through the above mechanism, AutoMerge can filter out most outliers.

IV. INCREMENTAL MERGING

For the large-scale merging task, we may encounter the case where there exists more than two groups of segments with overlaps. The overlaps between segments are limited at the early stage, and can be extended at the late stage. In the merging procedure, the manner used to divide all segments into different groups with stable connections is essential for incremental factor graph optimization. In this section, we will introduce the details of our incremental merging mechanism.

A. Multi-agent Clustering

Firstly, we formulate the incremental merging task into a traditional spectral clustering problem [43]. Assume there exists $V = \{v_1, \dots, v_n\}$ agents running in the real-time, and we can evaluate the inner connections between v_i and v_j as ω_{ij} . Without losing generality, we define a weighted graph $G = (V, E)$. E represents the edge connections, which satisfies $\omega_{ij} = \omega_{ji}$. We define $A_i, i = 1, \dots, k$ as the subset of V , and satisfies $A_1 \cup \dots \cup A_k = V, A_i \cap A_j = \emptyset, \bar{A}_i$ is the complement of A_i . And $W(A_i, \bar{A}_i)$ is weighted adjacency matrix, which is defined as,

$$W(A_i, \bar{A}_i) := \sum_{k \in A_i, l \in \bar{A}_i} \omega_{kl} \quad (8)$$

From the loop closure detection perspective, the inner connection ω_{ij} between agent v_i and v_j is based on overlap length and place recognition quality. Thus, we define inner connection ω_{ij} as,

$$\omega_{ij} = \begin{cases} \exp\left(-\frac{\|F_i - F_j\|_2^2 + C_w}{2L_{ij}^2 + \epsilon}\right), & i \neq j \\ 0, & i = j \end{cases} \quad (9)$$

where F_i indicates the extracted overlap place features from agent v_i , and L_{ij} is the length of overlap area. C_w is a hyper-parameter to control the ω_{ij} 's dependence on the overlaps'

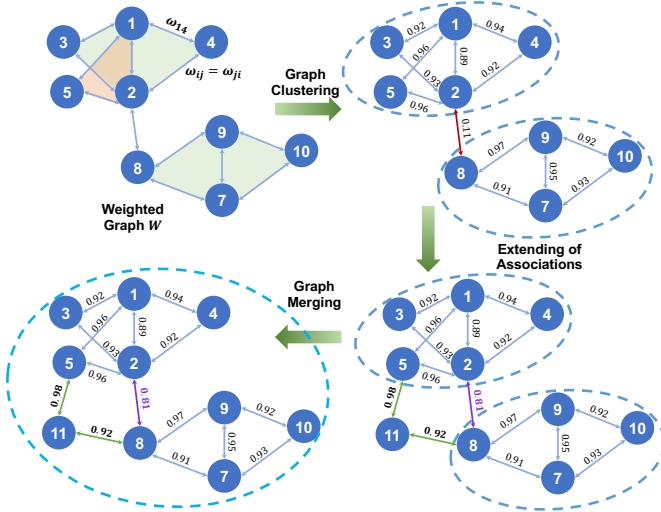


Fig. 5. **Incremental Merging.** (1) Graph $G = (V, E)$ is constructed with $V = \{v_1, \dots, v_n\}$ agents and their connections $\omega_{ij} \in E, i \neq j$. (2) AutoMerge can incrementally merge agents into different sub-groups by maximizing the inner connections within each sub-group and minimizing the connections between sub-groups. (3) When a new node v_{11} builds new confident connections with v_5 and v_8 , or previous connection $\omega_{2,8}$ is re-enhanced, AutoMerge can update the sub-groups into a joint group.

length, and $\epsilon = 1e - 4$ is a constant parameter. In the extreme cases where $\|F_i - F_j\|_2^2 \ll C_w$, the weighting $\omega_{ij} \sim \exp\left(-\frac{C_w}{2L_{ij}^2}\right)$ will mainly depend on the length of overlaps. Based on above equation, we can also define degree matrix D , where $d_{ii} = \sum_{j=1}^n \omega_{ij}$ and is the connection measurement between agent v_i with all other agents \bar{v}_i . According to spectral clustering [43], the incremental merging task can be defined as a mincut problem,

$$\min \text{cut}(A_1, \dots, A_k) := \min \frac{1}{2} \sum_{i=1}^k W(A_i, \bar{A}_i) \quad (10)$$

The major limitation of the above mincut is that it will simply separate one individual agent v_i from the rest of agents \bar{v}_i , which is not our desired map segmentation. To maintain sub-groups with a large size, we utilize the object function from Ncut [44],

$$\min \text{Ncut}(A_1, \dots, A_k) := \min \frac{1}{2} \sum_{i=1}^k \frac{W(A_i, \bar{A}_i)}{\text{vol}(A_i)} \quad (11)$$

$$\text{vol}(A_i) := \sum_{j \in A_i} d_{jj} \quad (12)$$

where $\text{vol}(A_i)$ is the measurement of inner connections among the sub-group A_i . From the power consumption perspective, incremental clustering is trying to find the best segment option with minimum penalty to divide the original agents into different consistent sub-groups.

The solution to the Ncut problem is detailed in the reference [43], and the standard spectral cluster approach as shown in Algorithm 1. Given the agent list $V = \{v_1, \dots, v_n\}$, we can calculate the similarity matrix (Eq. 9), degree matrix D , and corresponding Laplace matrix L . The eigenvalues

Algorithm 1 Incremental Clustering

Input: Agent list $V = \{v_1, \dots, v_n\}$

Output: Clusters A_1, \dots, A_k with $A_i \in \{j | y_j \in \mathcal{R}^k\}$

- 1: Construct similarity graph W , and ω_{ij} based Eq. 9
- 2: Construct degree matrix D , and $d_{ii} = \sum_{j=1}^n \omega_{ij}$
Calculate Laplace matrix $L = W - D$
- 4: Compute the eigenvectors $\mathcal{U} = \{u_1, \dots, u_n\}$ and eigenvalues $\{\lambda_1, \dots, \lambda_n\}$ from L
Sort eigenvectors \mathcal{U} based on eigenvalues
- 6: Determine the cluster numbers k based on $\lambda_{1, \dots, k} \leq \theta$
Construct key matrix $\mathcal{K} = \{u_1, \dots, u_k\}$, and get $y_i \in \mathcal{R}^k$ from i -th row from \mathcal{K}
- 8: Cluster points $(y_i)_{i=1, \dots, n}$ into k clusters with k -means.

$\lambda_k, k = 1, \dots, n$ can indicate the clustering status. In theory [43], if there exist k different sub-groups $\{A_1, \dots, A_k\}$ without connections $W(A_i, A_j) = 0, i \neq j$, the number of eigenvalues $\lambda_i = 0$ equals to k . In the map merging problem, partial overlaps between different sub-groups may exist, thus we set a control threshold ($\lambda_{max} \leq \theta$) to estimate the best sub-groups size. Based on the first k -dimension of eigenvectors \mathcal{U} , we can construct a key matrix $\mathcal{K}^{n \times k}$, and cluster to k classes though k -means. Through the above operation, AutoMerge can cluster agents into k sub-groups.

B. Incremental Merging

Recall that in Figure. 1, the data from different agents will stream to the AutoMerge server in random order. This procedure will require the loop closure detection to automatically find the potential overlaps between different agents, ignoring data-stream order. In the AutoMerge server system, each agent has its own identity (Agent-ID). As shown in Fig. 5, based on multi-agent clustering stated in Section. IV-A, the received agent lists $V = \{v_1, \dots, v_{10}\}$ can be clustered into 2 sub-groups $\{A_1, A_2\}$ based on their existing connections. When new observation for agent v_i received, AutoMerge will automatically estimate corresponding weightings $\omega_{ij}, i \neq j$ between v_i and $v_j \in \bar{v}_i$; when new overlaps are observed for existing agents, previous weak connection ($\omega_{2,8}$) is further enhanced. And based on updated global graphs, AutoMerge will merge original sub-groups into a joint graph. During the merging procedure, all of the different sub-graph are optimized through self-contained individual graph optimization.

V. DATASETS AND CRITERIA

To evaluate the map merging accuracy, we choose the well-known *KITTI* [13] dataset, one city-scale dataset collected in the City of Pittsburgh with around 120 km of trajectories in total, and one campus-scale dataset collected within Carnegie Mellon University with 4.5×8 km trajectories. The last two datasets are self-recorded with our data-collection platform, and they contain multiple revisits, as well as translation and orientation differences. In this section, we describe the datasets, target methods, and evaluation criteria.

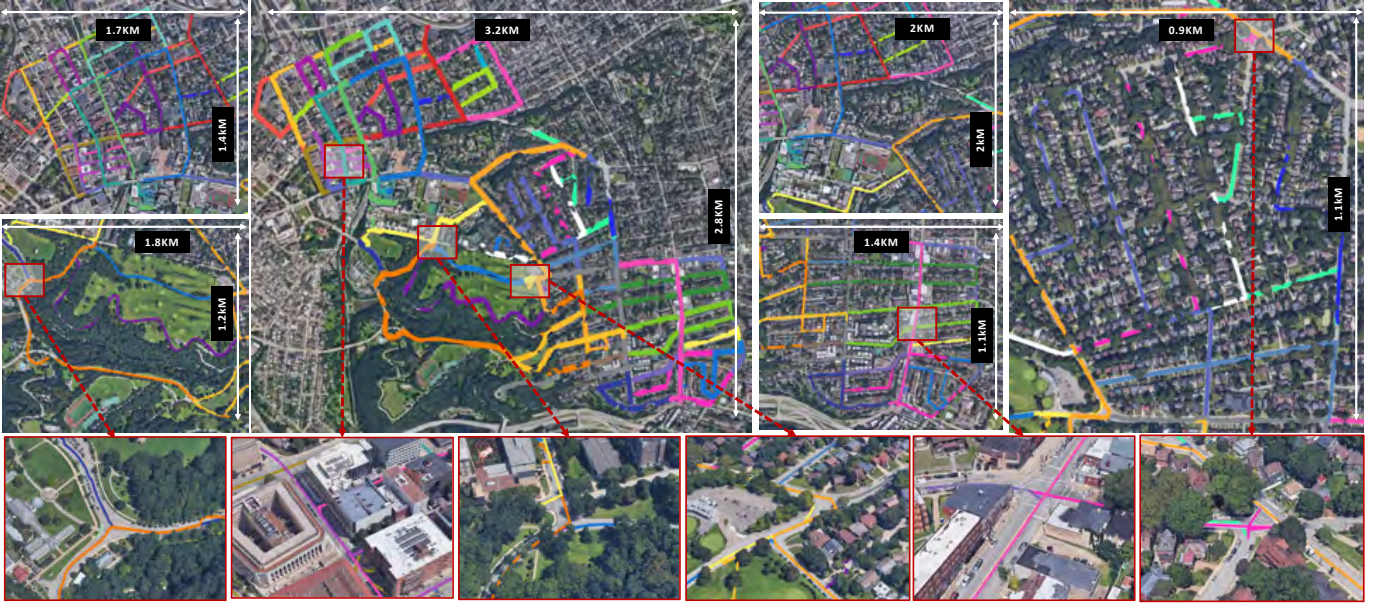


Fig. 6. **Self-collected Datasets.** Both *Pittsburgh* and *Campus* datasets are collected with our data-collection device (Velodyne-16 and Xsens MTI-300 IMU). The *Pittsburgh* dataset includes 5 zones (colored in green, yellow, red, yarn and blue), which covers street blocks, residential areas, parks, and commercial buildings. The *Campus* dataset is colored in purple, which covers the main campus area of Carnegie Mellon University.

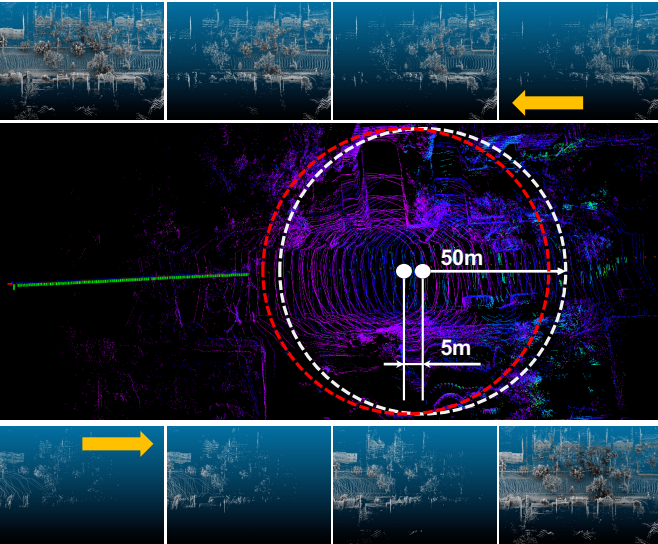


Fig. 7. **Sub-map Generation.** The dense maps are generated by accumulating the LiDAR scans into local sub-maps, which have a $50m$ radius and $5m$ offset from their neighbors. For either a forward or reverse traversal direction, the generated sub-maps for the same area share the similar geometric structures.

Merging Datasets: To cover various scenarios in our datasets, we travel through different types of areas over our self-gathered datasets, and we include multiple revisits. The detailed characteristics of each dataset and the environment will be provided in the following descriptions. Fig. 6 shows the overlaid segments on an aerial map, which illustrates the segment shapes, scales, and areas. The details are summarized in Table I.

- **Pittsburgh** dataset is collected within the city of Pittsburgh with our data-collection platform, which contains

TABLE I
COMPARISON OF DIFFERENT MAP MERGING APPROACHES.

Dataset	Environments	Scales (km)
KITTI [13]	Street	15×1
Pittsburgh	Street, Residential, Terrain	120×1
Campus	Campus area	4.5×8

a Velodyne-16 LiDAR scanner, Xsens MTI-300 inertial measurement units, and GNSS position systems. The collected areas (open street, residential areas, commercial buildings, etc.) contain 50 trajectories with a total distance of 120 km and 158 overlaps.

- **Campus** dataset is recorded with the same data-collection platform within the campus area of Carnegie Mellon University (CMU). The collected data covers 10 main trajectories throughout the campus, where each trajectory is recorded 8 times under different conditions (illuminations, directions, etc). The total length is around 36km.
- **KITTI** dataset is a well-known dataset for autonomous driving in urban environments. We extract out 10 (around 15km in total) trajectories from *KITTI* odometry dataset, and mainly used it to evaluate the generalization ability of our place recognition.

Due to sparse LiDAR scanning, occlusion, and changes in perspective, the same place may be represented by different observations. To provide consistent local maps for feature extraction, AutoMerge generates a dense map with traditional LiDAR odometry [40]. This approach has been applied in our previous work [6]. For each place, sub-maps are constructed by accumulating LiDAR scans into dense observations and keeping a distance (40m) to the vehicle's latest position. The sites in the CMU campus and *KITTI* datasets have a maximum of two lanes and large lateral displacement with no exceptions.

The sites in the Pittsburgh dataset street areas have two to four lanes, which indicates a certain lateral displacement during inverse observation. The major differences between the *Campus* dataset and the other datasets is the multiple revisits over the same segments. We extract sub-maps every 5m with a fixed 50m radius. Fig. 7 shows example extracted sub-maps. These maps can only be extracted when the relative distance between the vehicle’s central point and the keyframe’s is 100m away. In this manner, the geometric structures for the same areas will be very similar in both under forward and reverse traversal directions. The above datasets enable us to evaluate place recognition accuracy against rotational and lateral changes, refine data-association robustness against outlier wrong matches, and test map merging performance under large-scale environments. In all of the above datasets, we count the retrieval as successful if the detected candidates are 10m apart from the ground-truth positions.

Evaluation Criteria: To evaluate the loop closure detection accuracy and map merging performance, we use the following three metrics:

1) *Recalls@TopN Retrievals*: AutoMerge uses the best retrievals for map merging, and accurate place retrieval should be invariant to perspective differences. We utilize Top-1 recall as the main evaluation metric to analyze the place recognition robustness under changing viewpoints.

2) *Precision-Recall Curve*: recall cannot fully represent the general place recognition ability for global merging, as high false positives will make the map optimization fragile even with high recall. To this end, we utilize the precision-recall between different segments to investigate the accuracy of retrievals, and the generalization ability for unknown datasets.

3) *Merging Accuracy*: the above metrics mainly focus on fine-grained place recognition accuracy, and cannot fully encapsulate the performance in map-merging tasks. Since localization accuracy analysis (i.e., Mean Squared Error) is not realistic for large-scale merging, especially when odometry drift will be a part of the error, AutoMerge use a simplified merging metric. We notice that even limited accurate retrievals (2 ~ 4) on overlaps can provide accurate map merging results. For coarse-grained place retrieval accuracy, we care more about the overlaps’ binary retrieval rates, i.e., 0/1 for found/missed.

Targeting Methods: To analyze the place retrieval accuracy, we compare the fusion-enhanced descriptor extraction of AutoMerge with other state-of-the-art 3D place recognition methods: 1) M2DP [45] for non-learning based methods, and 2) PointNetVLAD [3], PCAN [46], LPDNet [29], SphereVLAD [35] for learning-based methods. In all the above methods, we use the same sub-map configuration, i.e. 5m distance between keyframes, and 50m radius and $0.5m^3$ voxelization for each sub-map as shown in Fig. 7. For map merging evaluation, we only use Top-1 retrieval to detect overlaps among segments, and apply *Merging Accuracy* to provide quantitative analysis and relative quality demonstration to investigate the merging details. Please note that point-based methods usually cannot find overlaps in the reverse

traversal direction (180°). For a fair comparison, we store the local features for both forward and reverse directions. Given the testing and reference queries, we calculate both distances ($\cos(f_{ref}^{forward}, f_{test}^{forward})$ and $\cos(f_{ref}^{forward}, f_{test}^{reverse})$), and use the minimum as the place feature distance.

To evaluate the generalization of the place recognition and data-association, we used only **30%** of the *Pittsburgh* dataset (which is **20%** of the total of all three datasets) to train different learning-based methods, and inference over the remaining datasets with the trained models.

VI. EXPERIMENTAL EVALUATION

As is shown in Table. I and Fig. 6, AutoMerge can work with multiple overlaps under city-scale and campus-scale environments, and under various types of scenarios. Overall, AutoMerge can achieve the best place recognition performance under varying viewpoint differences. And the map merging results also indicate that data association and incremental merging of AutoMerge are not sensitive to parameter tuning and demonstrate higher generalization potential for new environments. Comparing with other learning-based methods, AutoMerge still shows robust data association ability on all the datasets, even though only trained on *Pittsburgh* dataset. In this section, we will evaluate the place recognition accuracy, overlap retrieval accuracy, map merging efficiency, and computation efficiency respectively.

A. Place Recognition Results

1) *Orientation- and Translation- Tolerance Analysis*: We conduct experiments on three datasets to evaluate the robustness of place recognition of different methods. All learning-based methods are trained on tracks 1 ~ 15 of the Pittsburgh dataset. As shown in Fig. ??, we calculate the average Top-1 recall between query and reference frames (under translation differences $[1, 2, 3, 4]m$ and yaw orientation differences $[15, 30]^\circ$). To generate orientation differences, we rotate each query frame by a desired angle and then apply a random noise uniformly sampled from the range $-2.5^\circ \sim 2.5^\circ$. The projection-based methods, M2DP and SphereVLAD [35], can achieve orientation-invariance, but translation differences will greatly affect the recognition performance. Conversely, point-based methods can handle large translation differences but are sensitive to orientation differences. We can notice that AutoMerge has the translation-invariant property of point-based methods and orientation-invariant property of projection-based approaches. This is mainly due to our attention mechanism, which can reweigh the importance of the two branches in the feature extraction model.

On both the *KITTI* and *Pittsburgh* datasets, AutoMerge outperforms both point-based and projection-based methods when subjected to large orientation and translation differences. AutoMerge also shows great generalization compared to the single branch point-based and project-based approaches. We can also notice that, the non-learning method M2DP also shows accurate place recognition, especially on *KITTI* dataset. But the performance of M2DP will vary based on the 3D environments, which affects its map merging ability. In Fig. ??, we

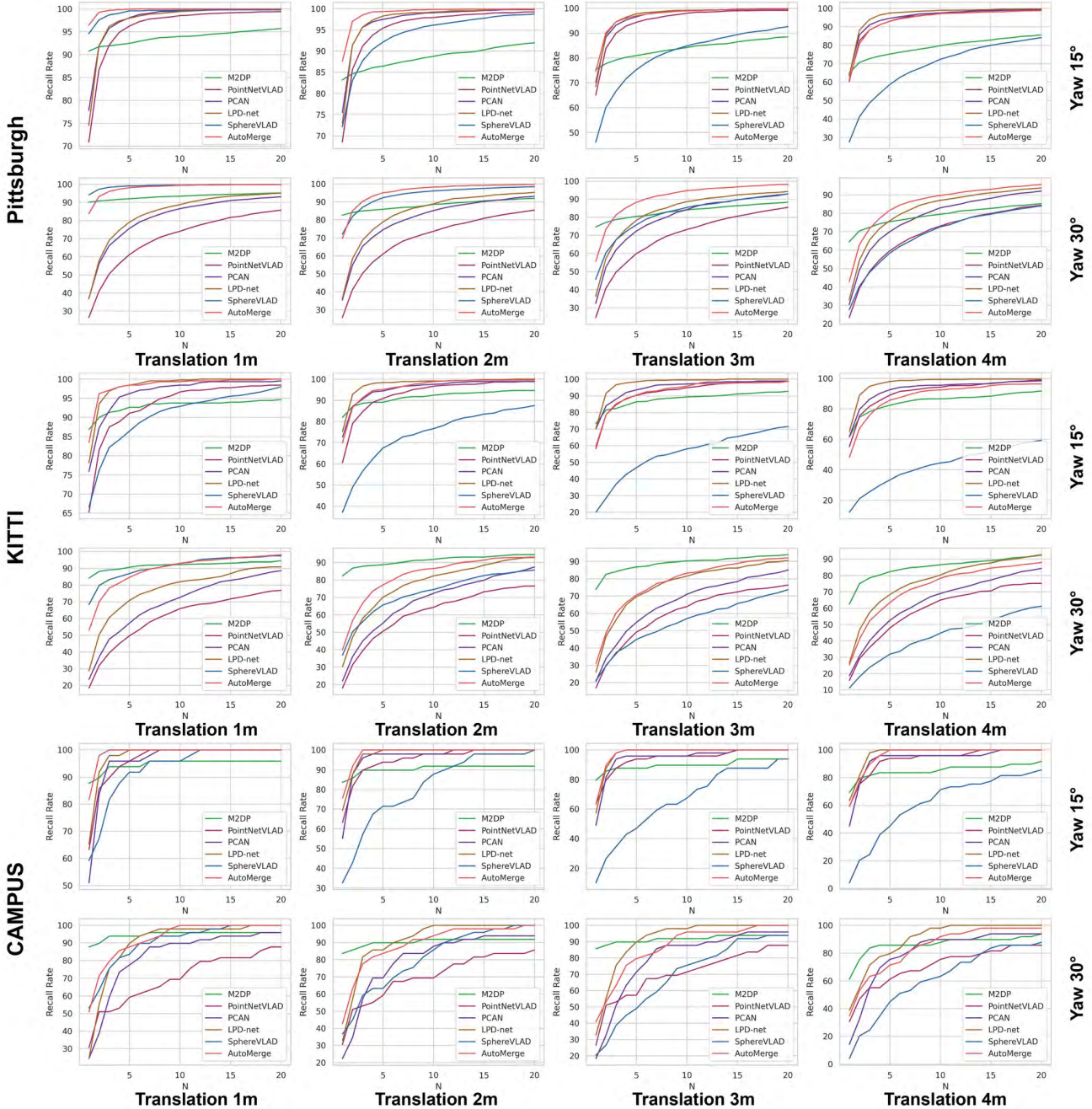


Fig. 8. **Localization results for different viewpoints on different datasets.** For each dataset, we pick one segment from the same domain and generate test/reference queries with different yaw angles $[15, 30]^\circ$ and translational displacement $[1, 2, 3, 4]m$, and then analyze the average recall for top-20 retrievals.

analyze the PR-curve of different methods over three datasets. We can notice that both SphereVLAD and AutoMerge show better performance than other descriptors. On the other hand, since all the methods are only trained on *Pittsburgh* dataset, there also exists general performances drop for all the learning-based approaches over the rest two datasets.

To investigate the merging ability, we analyze the merging accuracy over the *Pittsburgh* and *Campus* datasets. We extract out all the overlaps over the two datasets, and analyze the relative recalls and accuracy of the different methods. The

results are shown in Table.II. Non-learning method M2DP shows robust place recognition with high recall rates on one time visits. With generated viewpoint differences, it cannot provide accurate data association for different time observations. This is mainly because the LiDAR mapping varies over the different revisits. Even though we utilize the dense mapping mechanism to enhance the local sub-maps' consistency, there may still exist dynamic mapping noise and mapping density differences. Compared to non-learning methods, all learning-based approaches have higher generalization on both

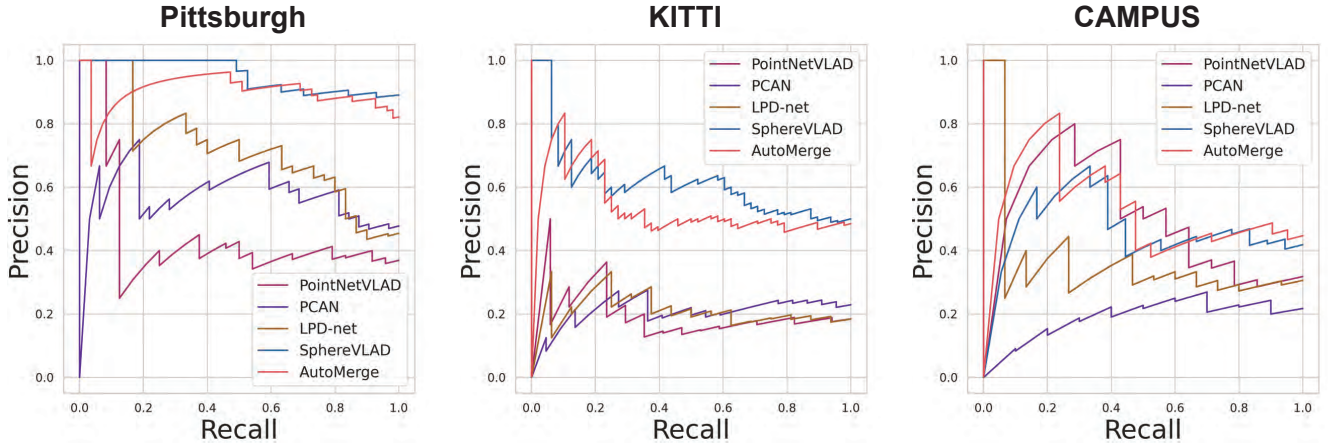


Fig. 9. **Precision-recall Curves (PR-curve) on three datasets.** On each dataset, the results are evaluated using testing and reference queries that have a relative translation of 3m and relative rotation of 10° .

TABLE II
MERGING ACCURACY ANALYSIS

Method	Pittsburgh		Campus	
	Precision	Recall	Precision	Recall
M2DP	80.5%	48.3%	90.5%	88.7%
PointNetVLAD	82.2%	31.4%	92.1%	87.4%
PCAN	82.6%	61.2%	94.6%	89.2%
LPD-Net	89.2%	65.3%	98.6%	90.3%
SphereVLAD	95.5%	72.0%	100.0%	93.5%
AutoMerge (ours)	93.7%	75.4%	100.0%	98.2%

datasets. And comparing with pure point- or projection- based approaches, AutoMerge shows higher precision and recall. This capability comes from the adaptive feature association, as stated in Section. II-B.

B. Map Merging

So far, we have investigated the place recognition results between paired segments. In this subsection, we consider the multi-segments offline/online map merging task on both the *Pittsburgh* and *Campus* datasets.

1) *Merging on Pittsburgh*: In offline merging, we assume all the segments of interest have already been recorded, and AutoMerge can obtain the poses and features over all trajectories at test time. Based on the relative connections among all the segments, AutoMerge can build the weighted graphs and cluster them into different sub-groups. In Fig. 10, we evaluate the merging performance over different zones of the *Pittsburgh* dataset. We can notice that sub-maps in each zone have converged into one consistent large map. However, not every segment has confident overlaps with other trajectories. Those segments with few interactions will be temporarily considered outliers. For areas with multiple segment overlaps, AutoMerge can also detect the potential connections while ignoring relative viewpoint differences. This property allows AutoMerge to have robust pose estimation with one-shot visits. As shown in Table. II, the merging performance is robust even in unknown environments. When tested on the *Pittsburgh* dataset, our model is trained on segments 1 ~ 10 giving it

13% dataset coverage. This training set only contains areas around Carnegie Mellon University. The final merging results do not show a significant performance drop over the rest of the datasets, which contains varying terrain, open streets, and residential areas. Because of its high generalization ability, AutoMerge does not require much data for training.

We also analyzed the robustness of offline clustering in the scenario where AutoMerge is given segments in a randomly selected order. In Fig. 11, we merged the segments for different values of parameter C_ω . For each parameter, we use a randomly generated 50 segment streaming order, and calculate the corresponding clustering trends. The results show that under all cases, AutoMerge can merge *Pittsburgh* segments into 6 major clusters, and the biggest cluster contains 43 segments, as shown in Fig. 10. From this, we can notice that the final clusters are not affected by the segment streaming order and the constant parameter C_ω .

For incremental merging on the *Pittsburgh* dataset, we assume all the segments are streamed incrementally. In this case, at the early merging stage, we can only observe partial trajectories, and wrong matches are unavoidable with these short-term observations. Using the incremental clustering method depicted in Sec. IV-A, AutoMerge can incrementally update the cluster property among segments. Fig. 12 shows the incremental merging results over different maximum segment distances (300m ~ 2400m). Fig. 13 shows the total cluster size under different maximum segment distances. In the 300m and 600m cases, the clusters have primarily merged into one cluster. This is because AutoMerge cannot distinguish different sub-groups when all the connections are weak. Beginning at the 900m distance, partial local overlaps are detected, and all 50 segments are divided into 4 ~ 6 clusters during the merging procedure. However, we can notice that not all cases can be divided to 6 clusters as we observed in the offline version of this task. This is mainly caused by wrong connections between partial observations as indicated in Fig. 12. We highlight the wrong matches in red circles. These temporary outliers can break the global map as shown in the 1200m and 2100m cases. But such failures can be quickly recovered from as shown in



Fig. 10. **Offline Merging on the Pittsburgh Dataset.** The above map is merged using 43 retrieved segments with limited overlaps from the *Pittsburgh* dataset. We show examples of open-street areas (bounded in red), terrain areas (bounded in green), and residential areas (bounded in yellow).

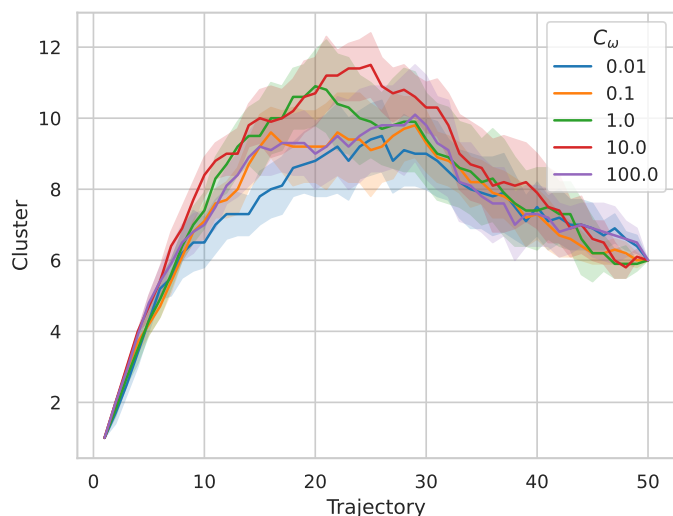


Fig. 11. **Incremental Clustering under Random Trajectory Order.** We evaluate the incremental clustering performance with different values for hyper-parameter C_ω , and we randomly order the trajectory sequences to incrementally update the graphs. For each C_ω , we evaluate the performance 100 times to analyze the merging trends.

the green circles in the 1500m and 2400m cases. In the above experiments we also analyze how the streaming order affects

merging for each maximum segment distance. The results show that AutoMerge’s clustering ability is invariant to the streaming order.

2) *Merging on Campus:* For the *Campus* dataset, we consider map merging in multi-session scenarios, where each area will be revisited multiple times, with the goal being achieving long-term autonomy. We chose 8 scenarios from the campus areas with sufficient temporal differences (from 3 ~ 5 days), and each trajectory is revisited 8 times with different traversal directions (forward/reverse) and illumination (day/night) conditions. As shown in Fig. 14, for each segment, we use a one-time visit as the reference map, and the rest of the visits as new queries. AutoMerge can automatically detect the loop closures between query and test keyframes through our invariant place descriptor and adaptive detection mechanism. Without any initial estimation, all segments over the same path are able to be transformed into one consistent map. The final refinements are conducted by Iterative Closet Point (ICP). However, due to dynamic objects and other sources of noise that occur in multiple visits, noisy merging will occur, especially in confined areas. This problem is most prevalent in segments 7 and 8, which contain lots of dynamic walking pedestrians within confined campus areas, and consequently the merged global map contains lots of merging noise. Improvements can be made by excluding dynamic objects and

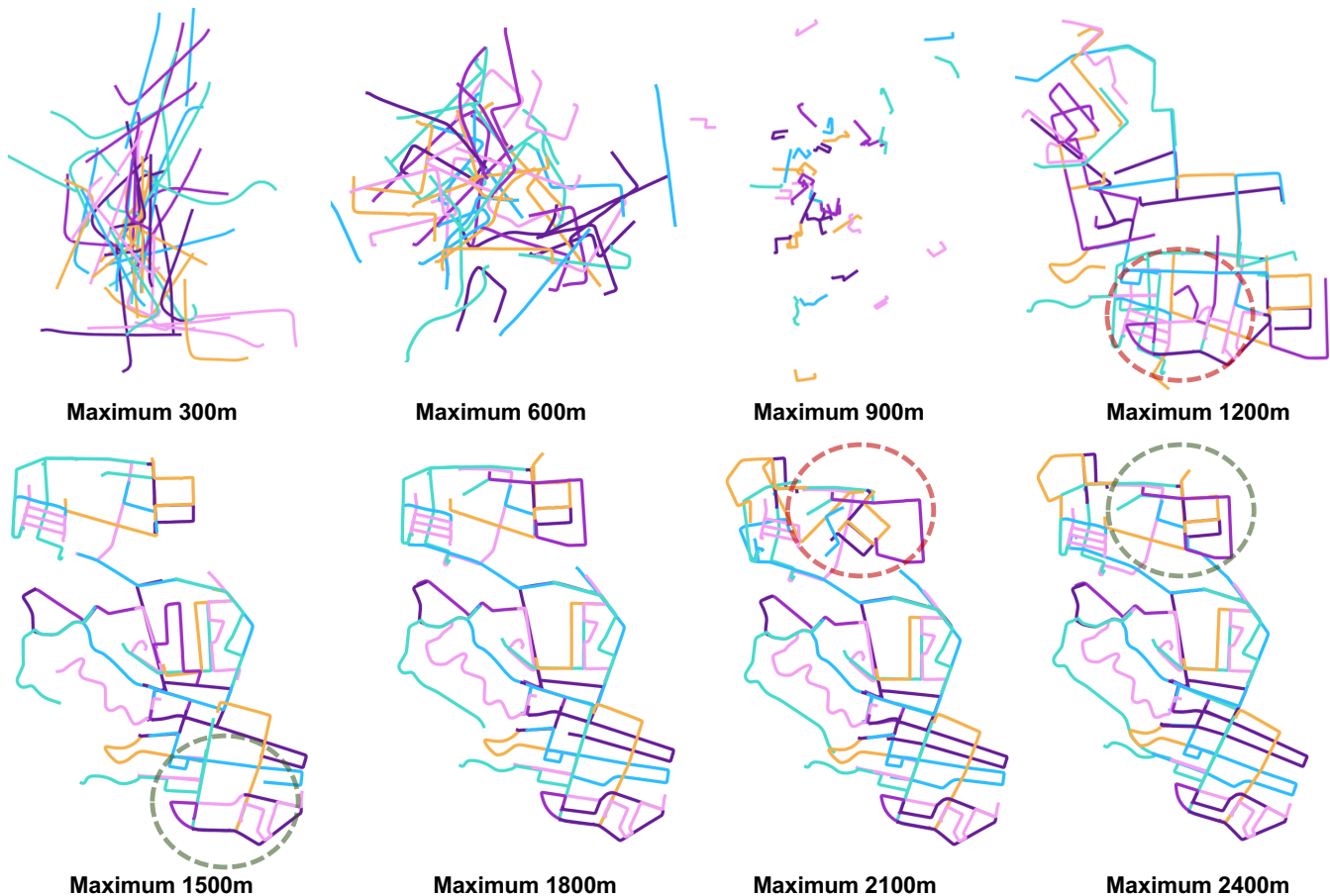


Fig. 12. **Map Merging with Incremental Expanding Trajectories.** This figure shows the incremental merging ability with different maximum segment length limitations, ranging from $300m$ to $2400m$. Failures due to incorrect matches are shown in red circles, and recovered/updated matches are shown in green circles. AutoMerge shows that it can recover when wrong matches occur during merging.

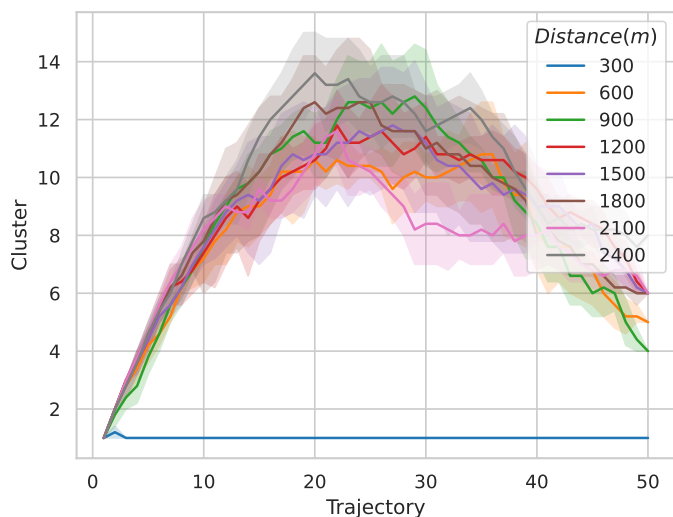


Fig. 13. **Online Clustering under Changing Distances.** We evaluate the incremental clustering performance under different maximum segment length limitations. For each distance, we evaluate the cluster results with 20 times random order.

using accurate General-ICP [25], but those methods require additional computation cost.

TABLE III
COMPARISON OF TIME, GPU MEMORY (MEGABYTE), AND FEATURE SIZE REQUIREMENTS OF DIFFERENT METHODS.

Method	GPU (MB)	Time (ms)	Feature Size
M2DP [45]	—	115.05	192
PointNetVLAD [3]	1,228	4.56	256
PCAN [46]	7,686	77.06	256
LPD-Net [29]	2,578	80.40	256
SphereVLAD [5]	1,069	2.81	512
AutoMerge (ours)	1,266	12.00	512

To better examine the merging performance in multi-session revisits, we visualize the data association for segment 1 as shown in Fig. 15. Different segments are drawn with different colors, and red links indicate the inner connections between them. To simplify the visualization, we did not draw all of the links between all of the pairs. The omnidirectional camera shows the appearances of the same area under different conditions. The bottom figures show the difference matrices when comparing the four test segments with one Forward-Day query segment. The stable data-association indicates the robustness of AutoMerge in multi-session revisits.

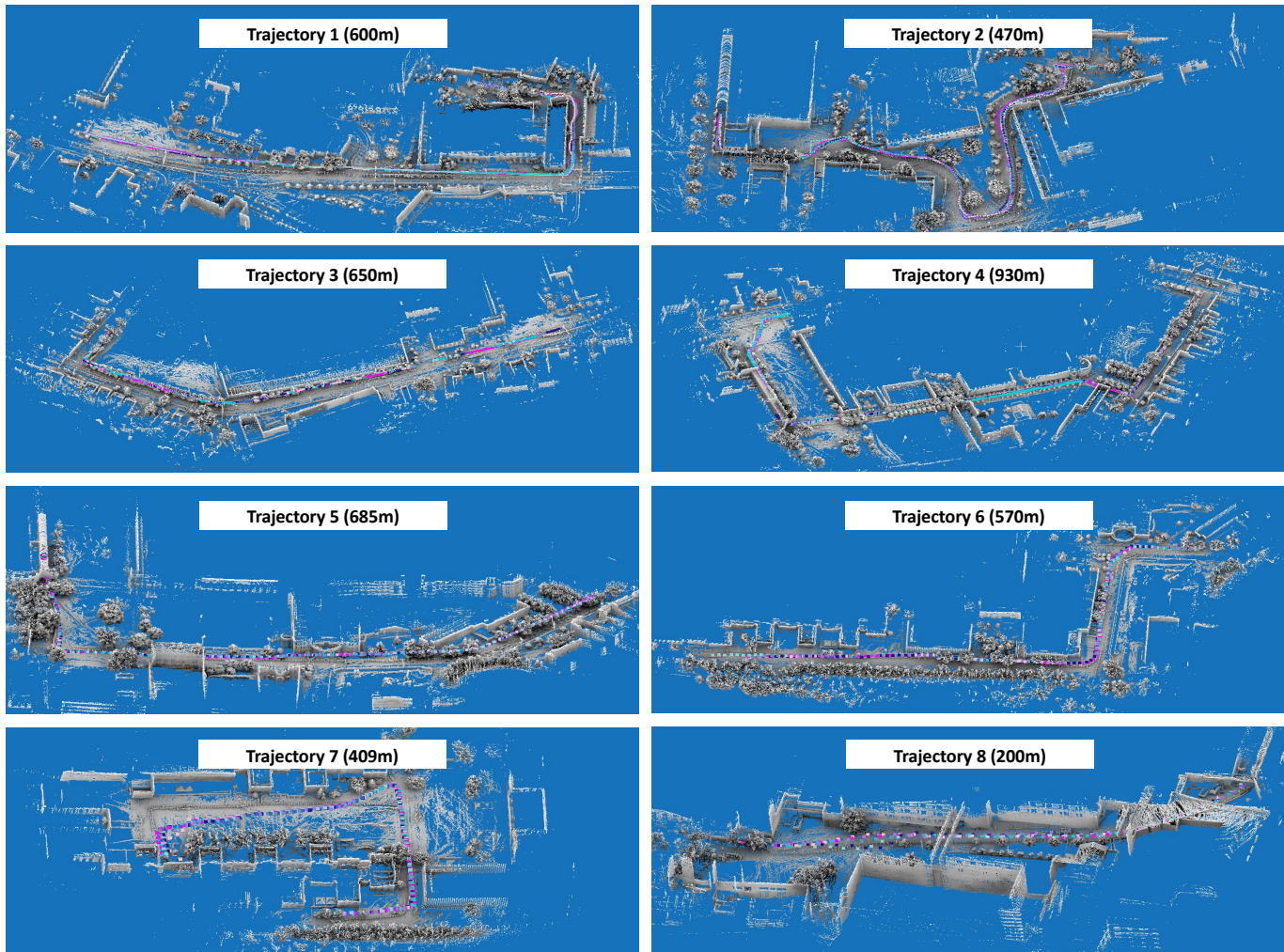


Fig. 14. **Merging over multiple revisits using the *Campus* dataset.** The robot revisits 8 different campus scenarios 8 times under different traversal directions and illuminations. The above subplots show the map merging results. The colored points indicate the merged segments from all visits.

C. Time and Storage Analysis

In this section, we compare the proposed method with the current state-of-the-art in learning-based 3D place recognition on both public and self-recorded datasets. To generate our datasets, we designed a data recording mobile platform. All the experiments are conducted on an Ubuntu 18.04 system with Nvidia RTX2060 GPU cards and 64G RAM. Table. III shows the memory usage, inference time and feature size for all the compared place descriptor methods. Compared with other methods, AutoMerge utilizes less GPU memory and has lower inference time with small storage requirements, which indicates that AutoMerge can be easily combined with current embedded systems.

We further investigate the time efficiency of the incremental merging procedure; in Fig. 16 we analyze the time usage during the incremental map merging for the *Pittsburgh* dataset. As we can see, with the AutoMerge framework, both feature extraction and map optimization are efficient, but data association is time-consuming. AutoMerge can infer a 5 ~ 10km trajectory within 2s, and optimize the global map within 0.5s, but data association time ranges from 4s

to 290s. This is mainly due to the computational complexity of sequence matching [10], which is $O(n^2)$ where n is the number of keyframes. The complexity increases with the reference map scale. Since the main procedure in sequence matching is the matrix multiplication operation, one solution for this problem is to apply CUDA-based sequence matching to reduce complexity.

VII. DISCUSSION & LIMITATIONS

As shown in the above analysis, AutoMerge can provide robust map merging for both city-scale and campus-scale environments without any initial estimation. This framework can provide both offline/online merging for single- and multi-agent systems, while ignoring viewpoint and temporal differences that are common in real-world mapping scenarios. However, AutoMerge also has the following limitations.

AutoMerge heavily utilizes generated dense local maps. Thus, the place recognition accuracy is determined by the stability of these local maps. As shown in Fig. 17, when the agent is moving too fast (red circle) or there exist too many dynamic objects (yellow circle), the noise and sparse

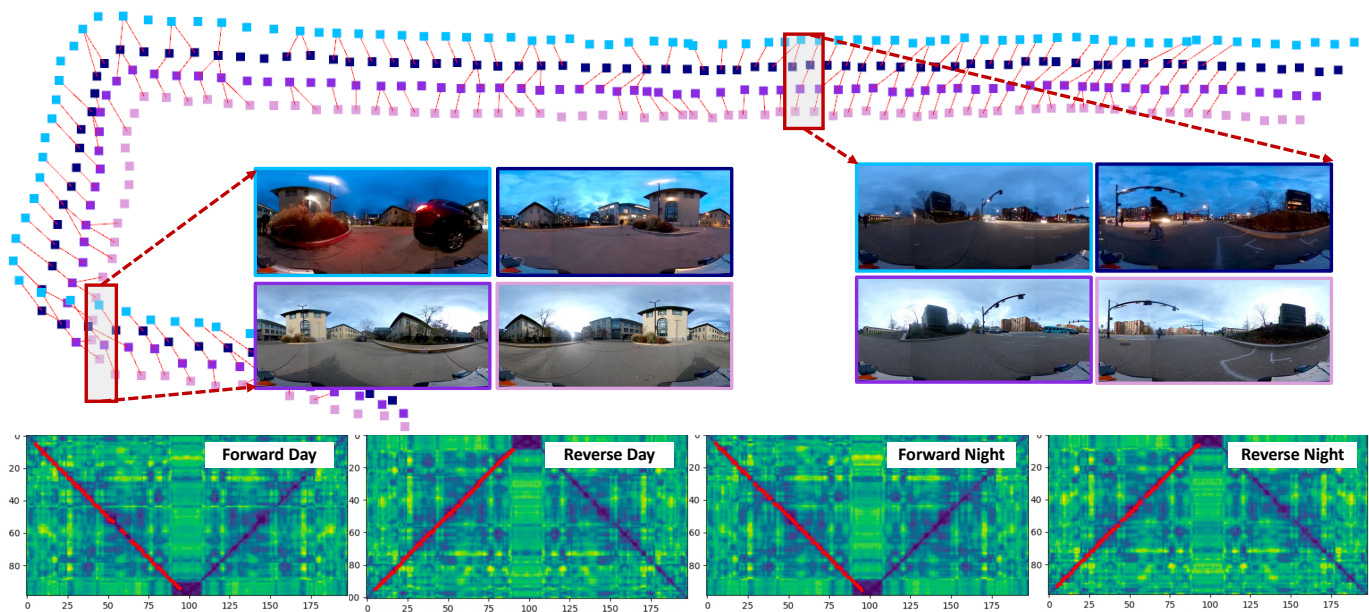


Fig. 15. **Data association on the Campus dataset.** Different segments are highlighted in different colors. For the same area we draw the relative data-association among keyframes. The omnidirectional camera images show the perspective differences over different revisits. The bottom figures show the difference matrices for all cases.

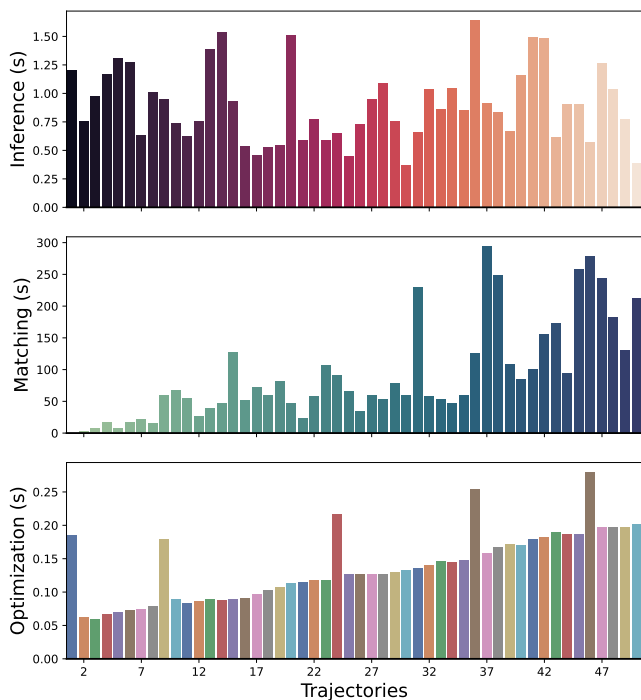


Fig. 16. **Efficiency and Storage Analysis for Pittsburgh dataset.** (i) The first row shows the inference time for the 50 segments – the distances for each segment range from $3km$ to $10km$. (ii) The second row shows the highest matching time; every new segment will try to match with all the previous queries. (iii) The third row shows the map optimization time.

local maps negatively impact the merging procedure. Such observations will introduce uncertainty in the extracted place descriptor, and indirectly affect the final merging performance.

Besides the noise and sparsity, the extracted place descriptor

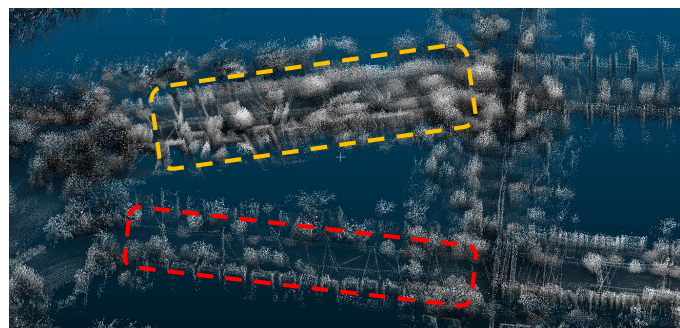


Fig. 17. **Noise and Sparse points in Map Merging.** The red circle shows the sparse local map when driving very fast. The yellow circle shows the noisy local map when encountering dynamic objects. These cases will introduce noise to the local place descriptor, which will affect the merging results.

is also sensitive to confined environments. In indoor areas, tunnels, and underground environments the generated LiDAR map is constrained within a relatively small space compared to outdoor environments. In these cases, distinguishable features cannot be easily extracted from either point-based or spherical projection-based data formats. To obtain rich geometries, point meshlization could be a potential solution.

Additionally, the adaptive loop closure detection is highly reliant on the sequence matching results, and subsequently, its sequence searching process is the most time-consuming part of AutoMerge. Since the main procedure in sequence matching is the brute-force searching operation, a CUDA-enhanced sequence matching mechanism can further improve searching efficiency, as mentioned in [47].

AutoMerge cannot handle trajectories with limited overlap. Since high merging accuracy is our primary goal, only high confidence overlaps are selected as loop closure candidates. The major drawback of this mechanism is missed loop closures

in trajectories with minimum overlap. These cases are usually encountered at crossroads where neighbor trajectories only have 1 ~ 2 matched keyframes. However, from the standpoint of large-scale merging performance, this principle is necessary, since we need to detect potential overlaps within hundreds of kilometers of trajectories; in such a scenario, several wrong short-range matches will crash the entire system.

Finally, the map merging ability of AutoMerge can be further extended with other types of sensors, such as new types of LiDAR sensors (solid-state LiDAR) and cameras (omnidirectional cameras). Because AutoMerge provides a map merging framework, any existing modules within AutoMerge can be replaced to fit the specific properties of other sensors.

VIII. CONCLUSIONS

In this paper we proposed AutoMerge, the first real-world automatic merging system for large-scale 3D mapping. Without using the initial positions of segments in the global frame, AutoMerge can automatically detect the relative overlaps between segments due to its viewpoint-invariant place recognition ability. In spite of the complicated cite-scale environments and similar-looking 3D areas under different scenarios, AutoMerge provides highly accurate data association with our adaptive loop closure detection module. Finally, by using the incremental merging module, AutoMerge can successfully merge sub-segments that are given in non-sequential order. The above properties make AutoMerge suitable to merge large-scale maps, such as cite-scale, campus-scale, and subterranean environments.

The results on both public and self-recorded datasets show our place retrieval ability notably outperforms all of the state-of-the-art methods in 3D loop closure detection. Because of its high recall rates and its incremental merging ability, AutoMerge seems like a promising method to use on various kinds of real-world datasets. Our method can work with limited computational resources and storage space, making it extremely suitable for low-cost robots in large-scale map merging tasks. In future works, we will target the current limitations of our method, and make this code publicly available.

REFERENCES

- [1] K. Ebadi, Y. Chang, M. Palieri, A. Stephens, A. Hatteland, E. Heiden, A. Thakur, N. Funabiki, B. Morrell, S. Wood, L. Carlone, and A. Agha-mohammadi, "Lamp: Large-scale autonomous mapping and positioning for exploration of perceptually-degraded subterranean environments," in *2020 IEEE International Conference on Robotics and Automation (ICRA)*, 2020, pp. 80–86.
- [2] J. G. Mangelson, D. Dominic, R. M. Eustice, and R. Vasudevan, "Pairwise consistent measurement set maximization for robust multi-robot map merging," in *2018 IEEE International Conference on Robotics and Automation (ICRA)*, 2018, pp. 2916–2923.
- [3] M. A. Uy and G. H. Lee, "Pointnetvlad: Deep point cloud based retrieval for large-scale place recognition," in *2018 IEEE/CVF Conference on Computer Vision and Pattern Recognition*, 2018, pp. 4470–4479.
- [4] X. Chen, T. Labe, A. Milioto, T. Rohling, O. Vysotska, A. Haag, J. Behley, and C. Stachniss, "OverlapNet: Loop Closing for LiDAR-based SLAM," in *Proceedings of Robotics: Science and Systems*, Corvallis, Oregon, USA, July 2020.
- [5] P. Yin, F. Wang, A. Egorov, J. Hou, Z. Jia, and J. Han, "Fast sequence-matching enhanced viewpoint-invariant 3-d place recognition," *IEEE Transactions on Industrial Electronics*, vol. 69, no. 2, pp. 2127–2135, 2022.
- [6] P. Yin, L. Xu, J. Zhang, and H. Choset, "Fusionvlad: A multi-view deep fusion networks for viewpoint-free 3d place recognition," *IEEE Robotics and Automation Letters*, vol. 6, no. 2, pp. 2304–2310, 2021.
- [7] A. Vaswani, N. Shazeer, N. Parmar, J. Uszkoreit, L. Jones, A. N. Gomez, . Kaiser, and I. Polosukhin, "Attention is all you need," *Advances in neural information processing systems*, vol. 30, 2017.
- [8] D. Galvez-Lopez and J. D. Tardos, "Bags of binary words for fast place recognition in image sequences," *IEEE Transactions on Robotics*, vol. 28, no. 5, pp. 1188–1197, 2012.
- [9] P. Yin, R. A. Srivatsan, Y. Chen, X. Li, H. Zhang, L. Xu, L. Li, Z. Jia, J. Ji, and Y. He, "Mrs-vpr: a multi-resolution sampling based global visual place recognition method," in *2019 International Conference on Robotics and Automation (ICRA)*, 2019, pp. 7137–7142.
- [10] M. J. Milford and G. F. Wyeth, "Seqslam: Visual route-based navigation for sunny summer days and stormy winter nights," in *2012 IEEE International Conference on Robotics and Automation*, 2012, pp. 1643–1649.
- [11] M. A. Fischler and R. C. Bolles, "Random sample consensus: A paradigm for model fitting with applications to image analysis and automated cartography," *Communications of the ACM*, vol. 24, no. 6, pp. 381–395, 1981.
- [12] S. Choi, Q.-Y. Zhou, and V. Koltun, "Robust reconstruction of indoor scenes," in *2015 IEEE Conference on Computer Vision and Pattern Recognition (CVPR)*, 2015, pp. 5556–5565.
- [13] A. Geiger, P. Lenz, C. Stiller, and R. Urtasun, "Vision meets robotics: The kitti dataset," *The International Journal of Robotics Research*, vol. 32, no. 11, pp. 1231–1237, 2013.
- [14] H. Lai, P. Yin, and S. Scherer, "Adafusion: Visual-lidar fusion with adaptive weights for place recognition," 2021. [Online]. Available: <https://arxiv.org/abs/2111.11739>
- [15] Y. Tian, Y. Chang, F. H. Arias, C. Nieto-Granda, J. P. How, and L. Carlone, "Kimera-multi: Robust, distributed, dense metric-semantic slam for multi-robot systems," *IEEE Transactions on Robotics*, pp. 1–17, 2022.
- [16] L. Paull, S. Saeedi G, M. Seto, and H. Li, "A multi-agent framework with moos-ivp for autonomous underwater vehicles with sidescan sonar sensors," in *Autonomous and Intelligent Systems*, vol. 6752, 2011, pp. 41–50.
- [17] S. Lowry, N. Sunderhauf, P. Newman, J. J. Leonard, D. Cox, P. Corke, and M. J. Milford, "Visual place recognition: A survey," *IEEE Transactions on Robotics*, vol. 32, no. 1, pp. 1–19, 2016.
- [18] S. Carpin, "Fast and accurate map merging for multi-robot systems," *Autonomous Robots*, vol. 25, no. 3, pp. 305–316, OCT 2008.
- [19] M. Labbe and F. Michaud, "Rtab-map as an open-source lidar and visual simultaneous localization and mapping library for large-scale and long-term online operation," *Journal of Field Robotics*, vol. 36, no. 2, pp. 416–446, MAR 2019.
- [20] R. Dube, A. Cramariuc, D. Dugas, H. Sommer, M. Dymczyk, J. Nieto, R. Siegwart, and C. Cadena, "Segmap: Segment-based mapping and localization using data-driven descriptors," *International Journal of Robotics Research*, vol. 39, no. 2-3, SI, pp. 339–355, MAR 2020.
- [21] A. Yang, Y. Luo, L. Chen, and Y. Xu, "Survey of 3d map in slam: Localization and navigation," in *Advanced Computational Methods in Life System Modeling and Simulation, LSMS 2017, PT I*, ser. Communications in Computer and Information Science, vol. 761, 2017, pp. 410–420.
- [22] A. Hornung, K. M. Wurm, M. Bennewitz, C. Stachniss, and W. Burgard, "Octomap: An efficient probabilistic 3d mapping framework based on octrees," *Autonomous Robots*, vol. 34, no. 3, pp. 189–206, APR 2013.
- [23] A. Rosinol, A. Violette, M. Abate, N. Hughes, Y. Chang, J. Shi, A. Gupta, and L. Carlone, "Kimera: From slam to spatial perception with 3d dynamic scene graphs," *The International Journal of Robotics Research*, vol. 40, no. 12-14, SI, pp. 1510–1546, 2021.
- [24] S. Rusinkiewicz and M. Levoy, "Efficient variants of the icp algorithm," in *Proceedings Third International Conference on 3-D Digital Imaging and Modeling*, 2001, pp. 145–152.
- [25] A. Segal, D. Haehnel, and S. Thrun, "Generalized-icp," in *Proceedings of Robotics: Science and Systems*, Seattle, USA, June 2009.
- [26] C. R. Qi, H. Su, K. Mo, and L. J. Guibas, "Pointnet: Deep learning on point sets for 3d classification and segmentation," in *Proceedings of the IEEE conference on computer vision and pattern recognition*, 2017, pp. 652–660.
- [27] R. Arandjelovic, P. Gronat, A. Torii, T. Pajdla, and J. Sivic, "Netvlad: Cnn architecture for weakly supervised place recognition," in *Proceedings of the IEEE conference on computer vision and pattern recognition*, vol. 40, no. 6, 2018, pp. 1437–1451.
- [28] C. R. Qi, L. Yi, H. Su, and L. J. Guibas, "Pointnet++: Deep hierarchical feature learning on point sets in a metric space," in *Advances in neural*

information processing systems (NIPS 2017), vol. 30, 2017, pp. 5099–5108.

- [29] Z. Liu, S. Zhou, C. Suo, P. Yin, W. Chen, H. Wang, H. Li, and Y. Liu, “Lpd-net: 3d point cloud learning for large-scale place recognition and environment analysis,” in *2019 IEEE/CVF International Conference on Computer Vision (ICCV)*, 2019, pp. 2831–2840.
- [30] W. Wohlkinger and M. Vincze, “Ensemble of shape functions for 3d object classification,” in *2011 IEEE International Conference on Robotics and Biomimetics*, 2011, pp. 2987–2992.
- [31] C. Esteves, C. Allen-Blanchette, A. Makadia, and K. Daniilidis, “Learning so (3) equivariant representations with spherical cnns,” in *Proceedings of the European Conference on Computer Vision (ECCV)*, 2018, pp. 52–68.
- [32] G. Kim, S. Choi, and A. Kim, “Scan context++: Structural place recognition robust to rotation and lateral variations in urban environments,” *IEEE Transactions on Robotics*, pp. 1–19, 2021.
- [33] F. Tombari, S. Salti, and L. Di Stefano, “Unique signatures of histograms for local surface description,” in *Computer Vision-ECCV 2010, PT III*, ser. Lecture Notes in Computer Science, vol. 6313, no. III, 2010, pp. 356–369.
- [34] P. Yin, L. Xu, Z. Liu, L. Li, H. Salman, Y. He, W. Xu, H. Wang, and H. Choset, “Stabilize an unsupervised feature learning for lidar-based place recognition,” in *2018 IEEE/RSJ International Conference on Intelligent Robots and Systems (IROS)*, 2018, pp. 1162–1167.
- [35] P. Yin, F. Wang, A. Egorov, J. Hou, J. Zhang, and H. Choset, “Seqspherevlad: Sequence matching enhanced orientation-invariant place recognition,” in *2020 IEEE/RSJ International Conference on Intelligent Robots and Systems (IROS)*, 2020, pp. 5024–5029.
- [36] L. Hui, M. Cheng, J. Xie, J. Yang, and M.-M. Cheng, “Efficient 3d point cloud feature learning for large-scale place recognition,” *IEEE Transactions on Image Processing*, vol. 31, pp. 1258–1270, 2022.
- [37] J. Ma, J. Zhang, J. Xu, R. Ai, W. Gu, C. Stachniss, and X. Chen, “Overlaptransformer: An efficient and rotation-invariant transformer network for lidar-based place recognition,” 2022. [Online]. Available: <https://arxiv.org/abs/2203.03397>
- [38] R. Arandjelovic and A. Zisserman, “All about vlad,” in *2013 IEEE Conference on Computer Vision and Pattern Recognition*, 2013, pp. 1578–1585.
- [39] T. Shan, B. Englot, F. Duarte, C. Ratti, and D. Rus, “Robust place recognition using an imaging lidar,” in *2021 IEEE International Conference on Robotics and Automation (ICRA)*, 2021, pp. 5469–5475.
- [40] J. Zhang and S. Singh, “Loam: Lidar odometry and mapping in real-time,” in *Proceedings of Robotics: Science and Systems*, Berkeley, USA, July 2014.
- [41] J. Fu, J. Liu, H. Tian, Y. Li, Y. Bao, Z. Fang, and H. Lu, “Dual attention network for scene segmentation,” in *2019 IEEE/CVF Conference on Computer Vision and Pattern Recognition (CVPR)*, 2019, pp. 3141–3149.
- [42] W. Ma, J. Zhao, H. Zhu, J. Shen, L. Jiao, Y. Wu, and B. Hou, “A spatial-channel collaborative attention network for enhancement of multiresolution classification,” *Remote Sensing*, vol. 13, no. 1, p. 106, 2020.
- [43] U. Von Luxburg, “A tutorial on spectral clustering,” *Statistics and Computing*, vol. 17, no. 4, pp. 395–416, Dec 2007.
- [44] J. Shi and J. Malik, “Normalized cuts and image segmentation,” *IEEE Transactions on Pattern Analysis and Machine Intelligence*, vol. 22, no. 8, pp. 888–905, 2000.
- [45] L. He, X. Wang, and H. Zhang, “M2dp: A novel 3d point cloud descriptor and its application in loop closure detection,” in *2016 IEEE/RSJ International Conference on Intelligent Robots and Systems (IROS)*, 2016, pp. 231–237.
- [46] W. Zhang and C. Xiao, “Pcan: 3d attention map learning using contextual information for point cloud based retrieval,” in *2019 IEEE/CVF Conference on Computer Vision and Pattern Recognition (CVPR)*, 2019, pp. 12428–12437.
- [47] S. Ouerghi, R. Boutteau, F. Tlili, and X. Savatier, “Cuda-based seqslam for real-time place recognition,” in *25. International Conference in Central Europe on Computer Graphics, Visualization and Computer Vision (WSCG 2017)*, ser. Computer Science Research Notes, vol. 2702, 2017, pp. 131–138.



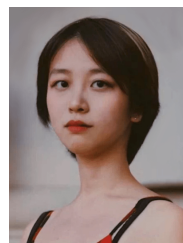
Peng Yin received his Bachelor’s degree from Harbin Institute of Technology, Harbin, China, in 2013, and his Ph.D. degree from the University of Chinese Academy of Sciences, Beijing, in 2018. He is a Post-doctoral researcher with the Robotics Institute at Carnegie Mellon University, Pittsburgh, USA. His research interests include LiDAR SLAM, Place Recognition, 3D Perception, and Reinforcement Learning. Dr. Yin has served as a Reviewer for several IEEE Conferences ICRA, IROS, ACC, RSS.



Haowen Lai received his B.E. degree in control science and engineering from Tongji University, Shanghai, China, in 2019. He is currently pursuing an M.S. degree from Tsinghua University, Beijing, China. His research mainly covers 3D localization and perception, SLAM, Place Recognition, and their application in robotics. He is trying to apply computer vision and machine learning techniques to robotics so as to make robots more intelligent in understanding the environment.



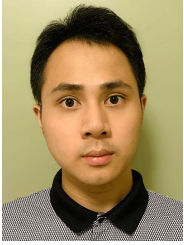
Shiqi Zhao received his Bachelor’s degree from Dalian University of Technology, Dalian, China, in 2018, and his Master’s degree from the University of California San Diego, U.S., in 2020. He is currently working as an intern at the Robotics Institute at Carnegie Mellon University. His research interests include Place Recognition, 3D Perception, and Deep Learning.



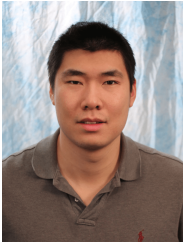
Ruijie Fu was born in Xi’an, China in 1999. She received her Bachelor’s of Science degree in Mathematics in 2020 from Carnegie Mellon University, Pittsburgh PA, USA, where she is currently working toward an M.S. degree in robotics. Her research interests include differential geometry and robot localization.



Ivan Cisneros received his B.S. degree in Electrical Engineering with a minor in Computer Science from Harvard University in 2016. He worked full time at NASA-JPL on several flight projects for 3 years before starting his graduate studies at Carnegie Mellon University. He is currently working on a Master’s degree in Robotics within the Robotics Institute at CMU. His research interests include SLAM, visual localization, 3D Perception, and deep learning.



Ruohai Ge received his B.S. degree in Electrical Engineering with a double major in Robotics from Carnegie Mellon University in 2016. He is currently working on a Master's degree in Robotics within the Robotics Institute at Carnegie Mellon University. His research interests include visual localization and robotic related software infrastructure.



Ji Zhang received his Ph.D. in Robotics from Carnegie Mellon University in 2017. Ji Zhang is a Systems Scientist at the Robotics Institute at Carnegie Mellon University, where he leads in the development of a series of autonomous navigation algorithms. His work was ranked #1 on the odometry leaderboard of KITTI Vision Benchmark between 2014 and 2021. He founded Kaarta, Inc, a CMU spin-off commercializing 3D mapping & modeling technologies, and stayed with the company for 4 years as chief scientist. His research interests are in robotic navigation, spanning localization, mapping, planning, and exploration.



Howie Choset received his B.S. Eng. degree in computer science and his B.S. Econ. degree in entrepreneurial management from the University of Pennsylvania (Wharton), Philadelphia, PA, USA, in 1990. He received M.S. and Ph.D. degrees in mechanical engineering from California Institute of Technology (Caltech), Pasadena, CA, USA, in 1991 and 1996, respectively. He is currently a Professor of Robotics at Carnegie Mellon University, Pittsburgh, PA, USA. His research group reduces complicated high dimensional problems found in robotics to low-dimensional simpler ones for design, analysis, and planning.



Sebastian Scherer received his B.S. in Computer Science, M.S. and Ph.D. in Robotics from CMU in 2004, 2007, and 2010. Sebastian Scherer is an Associate Research Professor at the Robotics Institute at Carnegie Mellon University. His research focuses on enabling autonomy for unmanned rotorcraft to operate at low altitude in cluttered environments. He is a Siebel scholar and a recipient of multiple paper awards and nominations, including AIAA@Infotech 2010 and FSR 2013. His research has been covered by the national and internal press including IEEE Spectrum, the New Scientist, Wired, der Spiegel, and the WSJ.